(Online) ISSN 2712-0562
*Original Research*

**Sustainable Engineering and Innovation**
Vol. 8, No. 2, 2026, pp.123-144
https://doi.org/10.37868/sei.v8i2.id1020

# Digital and bioinspired approaches to designing sustainable educational spaces: Modeling, optimization, and adaptive systems

**Aida Anafina[1*], Alla Kornilova[2]**
[1,2] Department, S. Seifullin Kazakh Agrotechnical Research University, Republic of Kazakhstan

*Corresponding author E-mail: anafinaaida@gmail.com

Received Jun. 6, 2026
Revised Sep. 3, 2026
Accepted Sep. 14, 2026
Online Sep. 29, 2026

**Abstract**

This study presents a mathematically rigorous, digitally bio-inspired framework for sustainable educational space design. Integrating parametric Building Information Modeling (BIM), computational fluid dynamics (CFD), surrogate response modeling, bio-inspired multi-objective optimization, and interval type-2 fuzzy adaptive control, the methodology is applied to a prototypical 4,860 m² learning center governed by fifteen decision variables. The optimization formulation simultaneously minimizes energy use intensity, discomfort hours, operational carbon, acoustic penalty, and daylight deficiency while maximizing graph-based spatial flexibility. Evaluating genetic algorithms, self-adaptive particle swarm optimization (SAPSO), and ant colony optimization across hypervolume and composite sustainability indices, SAPSO proved optimal. It reduced energy use intensity from 154.2 to 93.7 kWh/m²·yr, operational carbon from 127.8 to 75.4 $kgCO_2e/m^2 \cdot yr$, thermal discomfort from 418 to 143 h/yr, and reverberation time from 0.92 to 0.59 s, while boosting useful daylight illuminance from 54% to 81%. Additionally, interval type-2 fuzzy control yielded a further 17.6% in daily energy savings over rule-based operations. Architecturally interpreted through spatial typology, circulation, acoustic privacy, and user experience, the mathematical engine directly informs spatial design without supplanting human architectural judgment.

© The Author 2026.
Published by ARDA.

*Keywords*: Sustainable educational spaces, Digital twin, Bioinspired optimization, Entropy weighting, Interval type-2 fuzzy control, Alpha-cut uncertainty, TOPSIS

## 1. Introduction

In the present context, educational buildings are increasingly being viewed as low-carbon infrastructure, digitally enabled learning platforms, and healthy internal environments. The classroom or laboratory is no longer a room with a prescribed area. It is an interactive system in which thermal comfort, air quality, daylight, acoustics, digital connectivity, flexibility, and pedagogic experience interact.

Sustainable Development Goal 4 (SDG-4) on quality education is inherently linked to Sustainable Development Goal 11 (SDG-11) on sustainable cities and communities [1]. It is also relevant to engineering practice, as

This work is licensed under a Creative Commons Attribution License (https://creativecommons.org/licenses/by/4.0/ ) that allows others to share and adapt the material for any purpose (even commercially), in any medium with an acknowledgement of the work's authorship and initial publication in this journal.

decisions made at the planning stage significantly influence operational energy use and carbon emissions, as well as the long-term adaptability of buildings.

According to recent literature in educational technology, augmented educational reality and its accompanying immersive tools are changing how we teach and learn [2]. Studies on virtual reality in education also show that digital learning environments must be evaluated with ethical, social, and accessibility considerations [3]. These developments suggest that future learning spaces must accommodate on-site, immersive, and digitally mediated delivery. Therefore, sustainable educational-space design should consider both physical comfort and digital availability.

This study introduces a quantitative framework that presents the key design and operational variables as explicit mathematical relationships. The objective function has been derived from heat balance, carbon-dioxide balance, daylight utility, acoustic response, graph-based spatial flexibility, and an entropy weighting and TOPSIS closeness (fuzzy) optimization objectives as an optimization exercise de-abstracted from theoretical algorithms. In this updated conceptualization, every equation can be traced back to an architectural decision (i.e., proportion of a facade plane, the depth of a section, adjacency of classrooms, acoustic zoning permeability on daylighting penetration, and how much flexibility is useful for students and teachers).

This is because educational spaces are full of competing goals. For example, a larger glazing ratio may improve daylight but increase cooling load; high ventilation rates may reduce CO2 concentrations but increase fan and cooling energy use; more open spatial layouts may support flexible pedagogy but reduce acoustic clarity.

The research objectives are: (i) to formulate a mathematically explicit framework for sustainable educational-space optimization; (ii) to compare GA, PSO, and ACO under identical numerical budgets; (iii) to quantify design-stage and operation-stage performance improvements; and (iv) to demonstrate how fuzzy and bioinspired methods can support intelligent, human-centered, and sustainable educational environments. In addition, the study aims to derive architectural conclusions for spatial typology, user comfort, adaptable pedagogy, and operationally responsive learning environments.

## 1.1. Literature review

### 1.1.1. Digital modeling and co-simulation in educational buildings

BIM-to-BEM workflows have become essential in contemporary sustainable design because they enable the transfer of geometry, schedules, material properties, and system assumptions from design models to energy simulation tools. Kamel and Memari reviewed BIM applications in energy simulation and identified tool interoperability as a central technical challenge [4].

Garcez et al. verified that reliable information exchange between modeling platforms is an important factor for BIMbased sustainability assessment [5]. Parn et al. highlighted the importance of BIM trajectories in post-design building operations and facilities management [6]. Li and Wen conducted a review of building energy modeling for control and operation, which pertains to the operational layer of this work [7].

Nguyen et al. examined simulation-based optimization methods for building-performance analysis and highlighted the need for integrated numerical evaluation [8]. Kheiri reviewed energy-efficient building geometry and envelope optimization, which is directly related to the envelope variables used here [9]. Zhang et al. showcased parametric daylighting and energy optimization for school buildings, motivating the analysis of performance of educational buildings related to this paper [10]. Ji et al. created a generative-design-based performance optimization framework for sustainable building design that underpins the computation search structure used in this study [11]. They offer an operational layer, beyond design-stage modeling, that connects the physical structure with anatomically informed sensor streams and computational models to show how performance changes in real life (and how it could be changed). Madubuike et al. address this gap; a recent study surveyed 55 digital twin applications in construction and found that there exists a critical need for frameworks ready to be implemented [12]. Omrany et al. give broad guidance on what digital twins are in construction and highlight their potential by allowing sustainability-focused building management [13]. Tagliabue et al. showed an example of digital twins' application for sustainability assessment in already built environments [14]. Backlund et al. focused on human-in-the-loop digital twins of modern higher-education buildings, which fits perfectly the learning-space context this study is done in [15].

### 1.1.2. Bioinspired optimization methods

Biologically inspired optimizers are a well-established, effective alternative to many deterministic search methods, owing to their ability to accommodate nonlinear responses, mixed discrete-continuous variables, and multiple objectives. Delgarm et al. utilized particle swarm optimization in multi-objective building energy performance, demonstrating its applicability to simulation-based design [16].

To balance energy performance and thermal comfort objectives, Delgarm et al. [17] also applied an artificial bee colony method. Hamdy et al. focused on multi-objective optimization algorithms for nearly zero-energy buildings and demonstrated that the choice of algorithm influences the final design quality [18]. Tuhus-Dubrow and Krarti used a genetic-algorithm approach for envelope design optimization, which supports the GA benchmark used in this paper [19].

Ciardiello et al. studied multi-objective shape and envelope optimization, confirming the relevance of early-stage geometry and envelope decisions [20]. Mendez Echenagucia et al. examined envelope optimization during the early design stage with heating, cooling, and lighting objectives [21]. Carlucci et al. applied NSGA-II to minimize thermal and visual discomfort in nearly zero-energy building design, showing the need to treat comfort and energy as coupled objectives [22].

This optimization problem is richer than standard office energy optimization when the focus is on educational buildings. Huang et al. used dynamic clustering and particle swarm optimization to benchmark the energy performance of school buildings [23]. Shaughnessy et al. reported that classroom ventilation rates are associated with student performance [24]. Turunen et al. examined indoor environmental quality in school buildings and its relation to student health and well-being [25].

Brink et al. reviewed indoor environmental conditions affecting academic achievement in higher-education classrooms [26]. Lee et al. studied students' learning performance in air-conditioned university teaching rooms and linked indoor environmental quality to learning outcomes [27]. Barrett et al. demonstrated the effect of classroom design on pupil learning using a holistic, multilevel analysis [28].

Palacios Temprano et al. proposed deployment of large-scale sensors in schools for indoor environmental quality and learning outcomes [29]. Thus, a suitable optimization model must integrate physical response equations with focused decision-analysis methods. The paper utilizes intra-frame and final rankings as ranking layers instead of substitutes for Pareto optimal search, incorporating entropy weighting and TOPSIS.

### 1.1.3. Adaptive building systems and fuzzy logic

Adaptive lighting, ventilation/HVAC control, and blind control can reduce energy consumption without compromising comfort. Gunay et al. designed and executed a logic control for building operations in adaptive lighting and blinds [30]. Caicedo and Pandharipande developed a daylight- and occupancy-adaptive lighting control system through iterative optimization [31].

Killian and Kozek summarized prior studies on model predictive control for buildings with energy efficiency potential, discussing interpretability, interdependence on many factors from human behavior to regulation and policies as current challenges [32]. Hou et al. presented an LSTM and deep reinforcement learning-based occupancy-driven HVAC control optimization method to deliver better air quality, thermal comfort, and energy efficiency [33]. Tangible forms that facility managers can inspect are important in educational building control, and fuzzy logic is one of the few approaches to do this. Morales Escobar et al. proposed an advanced context-driven fuzzy control method for HVAC management systems in buildings [34]. Abuhussain et al. developed an adaptive HVAC fuzzy controller approach that uses additional input parameters to improve thermal comfort management [35]. Beheshtikhoo et al. designed a type-2 fuzzy logic controller for smart-home energy management with integration of renewable energy and electric vehicles [36].

Chojecki et al. compared fuzzy controllers with classical PID controllers in HVAC equipment and emphasized practical energy-efficiency and comfort benefits [37]. Interval type-2 fuzzy logic is particularly suitable when sensor measurements, user preferences, and operating schedules are uncertain. Mendel and John explained the fundamental structure of type-2 fuzzy sets in a form suitable for engineering applications [38]. Karnik et al. developed the core formulation of type-2 fuzzy logic systems, including type reduction and rule aggregation [39]. The present study, therefore, extends the adaptive-control literature by linking interval type-2 fuzzy operation with BIM-based modeling, multi-objective bioinspired search, entropy-TOPSIS ranking, and alpha-cut robustness analysis for educational spaces.

### 1.2. Research gap

The literature contains separate advances in BIM modeling, energy simulation, bioinspired optimization, adaptive control, and fuzzy decision support. Yet, few studies offer such a unified framework that is mathematical, numerical, interpretable, and relevant in/around educational spaces. In particular, existing studies rarely show how the mathematical framework serves an architectural problem, how numerical results are interpreted through space, typology, and users, and how they finally lead to architectural design conclusions.

This paper closes this gap by integrating co-simulation, surrogate modeling, entropy-TOPSIS decision ranking, and combining all of these with alpha-cut uncertainty in a reliability analysis based on interval type-2 fuzzy operations. The architectural contribution is therefore the translation of computational outputs into design guidance for facade articulation, classroom clustering, circulation permeability, flexible partitions, and learner-centered environmental quality.

## 2. Research method

### 2.1. Case study and decision variables

The reference case has been developed as a 4-story learning center with a total gross floor area of 4860 m². The model consists of classrooms, collaborative studios, digital laboratories, reading commons, makerspaces, seminar spaces, and faculty support. The reference building is air-conditioning-dominated, in use during the daytime, and has a very strong timetable variability. Architecturally, this case represents a mid-sized contemporary learning typology in which classrooms, studios, laboratories, reading commons, makerspaces, and faculty areas are not isolated rooms but interdependent spatial units connected through circulation, shared services, and user movement patterns.

The numerical case is designed as a typical simulation-based scenario, rather than as a post-occupancy field-measurement tool. As such, the results demonstrate relative algorithmic and design performance under controlled assumptions, while calibration with measured campus data would be essential for field deployment.

$$x=[x_1,x_2,\ldots,x_{15}]^T, \tag{1}$$

where the variables represent window-to-wall ratio, shading depth, wall U-value, roof U-value, solar heat-gain coefficient, thermal mass index, outdoor-air rate, daylight dimming threshold, outdoor-air fraction, cooling setpoint, heating setpoint, absorption coefficient, corridor openness ratio, modular partition factor, and adaptive controller gain.

So, the variables are more than engineering inputs: they relate to architectural decisions about partial open vs complete envelope depth; daylight modulation, spatial massing and tone; acoustic absorption; corridor porosity; and additional support of changing pedagogical layouts by partitions. Table 1 shows the definition of the decision variables and their numerical bounds.

Table 1. Decision variables and numerical bounds

| Variable | Description | Lower bound | Upper bound | Unit |
|---|---|---|---|---|
| $x_1$ | Window-to-wall ratio | 0.20 | 0.55 | - |
| $x_2$ | External shading depth | 0.20 | 1.00 | m |
| $x_3$ | Wall U-value | 0.28 | 0.65 | W/m²K |
| $x_4$ | Roof U-value | 0.18 | 0.42 | W/m²K |
| $x_5$ | Solar heat-gain coefficient | 0.22 | 0.50 | - |
| $x_6$ | Thermal mass index | 0.60 | 1.40 | - |
| $x_7$ | Outdoor-air rate | 7.00 | 16.00 | L/s.person |
| $x_8$ | Dimming threshold | 250 | 450 | lux |
| $x_9$ | Outdoor-air fraction | 0.15 | 0.45 | - |
| $x_{10}$ | Cooling setpoint | 23.0 | 26.0 | °C |
| $x_{11}$ | Heating setpoint | 19.0 | 22.0 | °C |
| $x_{12}$ | Absorption coefficient | 0.25 | 0.85 | - |
| $x_{13}$ | Corridor openness | 0.30 | 0.80 | - |
| $x_{14}$ | Modular partition factor | 0.20 | 0.90 | - |
| $x_{15}$ | Adaptive control gain | 0.40 | 1.20 | - |

Figure 1 below presents the integrated workflow that connects parametric BIM, co-simulation, surrogate modeling, bioinspired optimization, along with adaptive control.

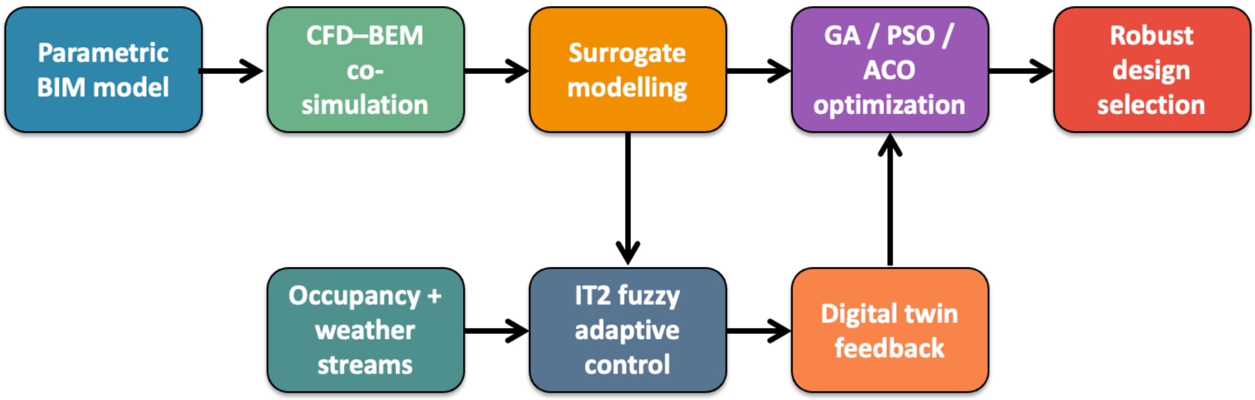


Figure 1. Integrated digital-bioinspired workflow used in the proposed study

## 2.2. Thermal and energy modeling

For each zone z, the reduced thermal balance is written as:

$$C_z \frac{dT_z(t)}{dt} = \sum_{j=1}^{n_e} U_j\, A_j\{T_o(t) - T_z(t)\} + \dot{m}_z c_p\{T_s(t) - T_z(t)\} + Q_{occ,z} + Q_{eq,z} + Q_{sol,z}. \qquad (2)$$

The solar gain entering zone $z$ is:

$$Q_{sol,z}(t) = \sum_{w=1}^{n_w} A_w\, \tau_w SHGC_w I_w(t)(1 - s_w). \qquad (3)$$

The annual energy use intensity is calculated as:

$$EUI = \frac{E_{heat}+E_{cool}+E_{light}+E_{vent}+E_{equip}}{A_f}, \qquad (4)$$

where $A_f = 4860m^2$. For the baseline case:

$$EUI_b = \frac{87.48+301.32+131.22+106.92+122.58}{4860} \times 1000 = 154.2 \text{ kWh/m}^2\text{yr}. \tag{5}$$

For the robust PSO design:

$$EUI_o = \frac{53.46+174.96+92.34+72.90+61.78}{4860} \times 1000 = 93.7 \text{ kWh/m}^2\text{yr2}. \tag{6}$$

The energy reduction percentage is therefore:

$$\Delta EUI = \frac{154.2-93.7}{154.2} \times 100 = 39.2\%. \tag{7}$$

### 2.3. Indoor air quality and carbon model

The carbon dioxide balance is expressed as:

$$\Delta V_z \frac{dC_z(t)}{dt} = G_z(t) + q_{oa,z}(t)\{C_o - C_z(t)\}. \tag{8}$$

The time-discretized form used in the simulation is:

$$C_z^{t+1} = C_z^t + \frac{\Delta t}{V_z}\left[G_z^t + q_{oa,z}^t(C_o - C_z^t)\right]. \tag{9}$$

The operational carbon intensity is:

$$CI = \frac{\sum_{r=1}^{R} E_r \gamma_r}{A_f}„ \tag{10}$$

where $\gamma_r$ is the emission factor of energy stream $r$.

The carbon improvement of the selected design is:

$$\Delta CI = \frac{127.8-75.4}{127.8} \times 100 = 41.0\%. \tag{11}$$

### 2.4. Thermal comfort, daylight, and acoustic equations

PMV and PPD represent thermal comfort. The numerical evaluation uses the standard functional relationship

Thermal comfort interpretation follows the ASHRAE Standard 55 guidance for human occupancy conditions [40].

The PMV-PPD relationship is consistent with the ISO 7730 guidance for analytical thermal comfort evaluation [41].

$$PPD = 100 - 95\exp[-0.03353PMV^4 - 0.2179PMV^2]. \tag{12}$$

The daylight metric follows the building-daylight principles specified in EN 17037 [42]. Useful daylight illuminance is calculated as:

$$UDI = 1/N\_occ \ \sum\_(t = 1)\hat{}(N\_occ)▒\delta \ (300 \le E\_t \le 3000) \times 100. \tag{13}$$

The acoustic reverberation time is estimated using the reverberation-time interpretation, which is aligned with ISO 3382-3 guidance on room-acoustic parameters [43]:

$$RT_{60} = \frac{0.161V}{\sum_i \alpha_i S_i}. \tag{14}$$

For a classroom with $V = 252\ m^3$ and equivalent absorption area $Aabs = 68.9\ m^2$, the optimized reverberation time is:

$$RT_{60,o} = \frac{0.161 \times 252}{68.9} = 0.589\ \text{s} \approx 0.59\ \text{s}. \tag{15}$$

### 2.5. Graph-based educational-space flexibility

Let $G = (V, E)$ be the adjacency graph of learning zones. The weighted flexibility score of zone $i$ is:

$$\phi_i = \eta_i \frac{deg(i)}{deg_{max}} + \mu_i \frac{a_i}{a_{max}} + \nu_i \frac{p_i}{p_{max}}. \tag{16}$$

The building-level spatial flexibility index is:

$$F_g = \frac{1}{|V|} \sum_{i=1}^{|V|} \phi_i. \tag{17}$$

Figure 2 below shows the representative learning-zone layout with sensor placement strategy and adjacency structure used for spatial flexibility analysis.

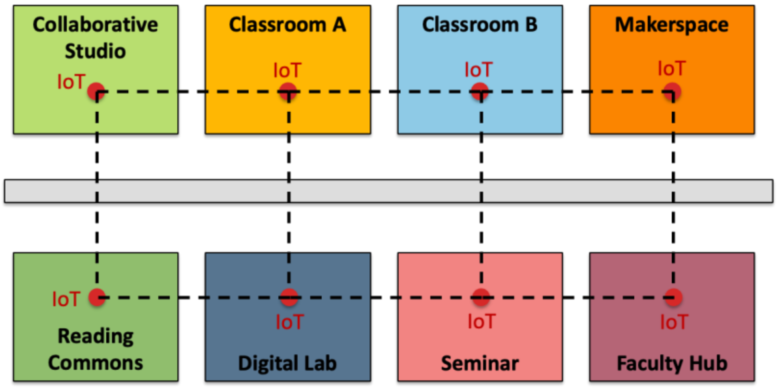


Figure 2. Zoning, sensor placement, and adjacency graph for the representative learning center

The adjacency graph visualized in Figure 2 is read out as an architectural typology of learning space. Nodes represent common spatial units, including classrooms, studios, laboratories, commons and seminar spaces or faculty hubs; edges represent circulation links through space, visual connection within and between spaces, shared access patterns across certain spaces (e.g. a classroom that is physically adjacent to a lab as creating opportunities for interactive learning), acoustic proximity or variability between linked areas and potential pedagogical pattern of interaction mediated by the adjacency. In this context, a high flexibility score refers to more than mere mathematical connectivity: it means that users may move through and interact within the learning center, reconfigure movement patterns, and occupy shared space without generating friction.

### 2.6. Surrogate modeling

The surrogate response for criterion k is expressed as:

$$\hat{f}_k(\mathbf{x}) = \beta_{0,k} + \sum_{i=1}^{15} \beta_{i,k}\, x_i + \sum_{i=1}^{15} \sum_{j=i}^{15} \beta_{ij,k}\, x_i x_j + \varepsilon_k(\mathbf{x}). \tag{18}$$

The prediction error statistics are:

$$RMSE_k = \sqrt{\frac{1}{n} \sum_{i=1}^{n} \left(f_{k,i} - \hat{f}_{k,i}\right)^2}; \tag{19}$$

$$R_k^2 = 1 - \frac{\sum_{i=1}^{n} \left(f_{k,i} - \hat{f}_{k,i}\right)^2}{\sum_{i=1}^{n} \left(f_{k,i} - \bar{f}_k\right)^2}. \tag{20}$$

Figure 3 validates the surrogate response model by comparison between simulated and surrogate-predicted EUI values.

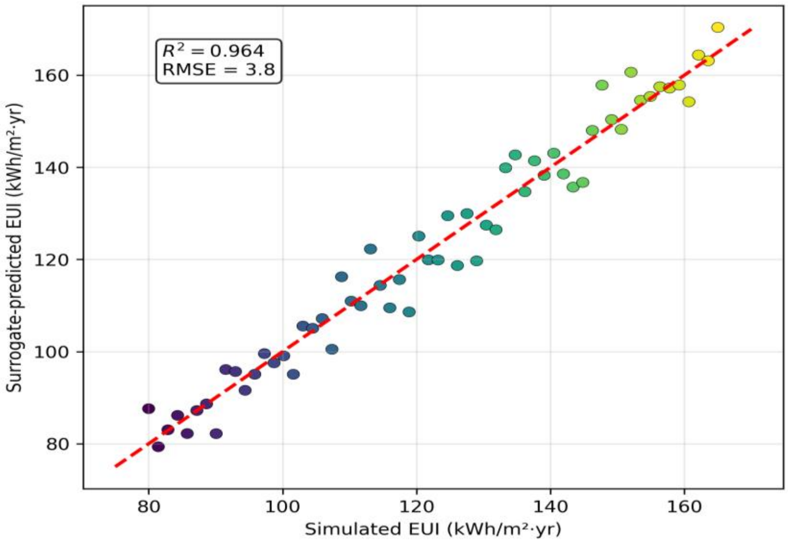


Figure 3. Surrogate validation for the physics-informed response model

Table 2 reports the surrogate model validation statistics used to assess prediction reliability.

Table 2. Decision variables and numerical bounds

| Response | $R^2$ | RMSE | MAE | Interpretation |
|---|---|---|---|---|
| EUI | 0.964 | 3.8 | 2.9 | Strong prediction |
| Discomfort hours | 0.951 | 21.4 | 16.8 | Acceptable for annual comfort |
| UDI | 0.944 | 2.7 | 2.1 | Strong daylight fit |
| RT60 | 0.958 | 0.034 | 0.026 | Strong acoustic fit |
| Carbon intensity | 0.969 | 2.9 | 2.2 | Strong carbon prediction |

### 2.7. Robust multi-objective optimization

NSGA-II is one of the most popular elitist reference structures for multi-objective evolutionary search [44]. The velocity-position update of PSO adheres to the classical particle-swarm formulation by Kennedy and Eberhart [45]. The ACO transition rule is based on the pheromone-learning structure used in cooperative search of [46]. Define ξ: uncertainty in weather and indoor environments, occupancy, internal gains, & uses of the timetable. Bi-Pod robustness response is given as:

$$\tilde{f}_k(\mathbf{x}) = \mathbb{E}_\xi[f_k(\mathbf{x}, \boldsymbol{\xi})] + \lambda_k \sigma_\xi[f_k(\mathbf{x}, \boldsymbol{\xi})]. \tag{21}$$

The multi-objective optimization model is:

$$\min_{\mathbf{x}\in\Omega} \mathbf{F}(\mathbf{x}) = \left[\widetilde{EUI}, \widetilde{DH}, \widetilde{CI}, \widetilde{RT}_{pen}, 1 - \widetilde{UDI}\right], \quad \max F_g(\mathbf{x}), \tag{22}$$

subject to:

$$-0.5 \le \overline{PMV} \le 0.5, \quad \overline{PPD} \le 10\%, \quad \overline{CO_2} \le 1000\ ppm, \quad RT_{60} \le 0.70\ s, \quad L_i \le x_i \le U_i. \tag{23}$$

The PSO update equations are:

$$\mathbf{v}_i^{t+1} = \omega \mathbf{v}_i^t + c_1 r_1 \left(\mathbf{p}_i^t - \mathbf{x}_i^t\right) + c_2 r_2 \left(\mathbf{g}^t - \mathbf{x}_i^t\right); \tag{24}$$

$$\mathbf{x}_i^{t+1} = \mathbf{x}_i^t + \mathbf{v}_i^{t+1}. \tag{25}$$

The GA offspring representation is:

$$\mathbf{x}_{child} = \theta \mathbf{x}_{parent1} + (1 - \theta)\mathbf{x}_{parent2} + \boldsymbol{\epsilon}_{mut}. \tag{26}$$

The ACO transition probability is:

$$P_{ij}^{(a)} = \frac{\tau_{ij}^{\alpha}\eta_{ij}^{\beta}}{\sum_{l\in\mathcal{N}_i}\tau_{il}^{\alpha}\eta_{il}^{\beta}}. \tag{27}$$

and the pheromone update is:

$$\tau_{ij}^{t+1} = (1-\rho)\tau_{ij}^{t} + \sum_a \Delta\,\tau_{ij}^{(a)}. \tag{28}$$

Figure 4 compares the Pareto-optimal solutions generated by GA, PSO, and ACO under the same search budget.

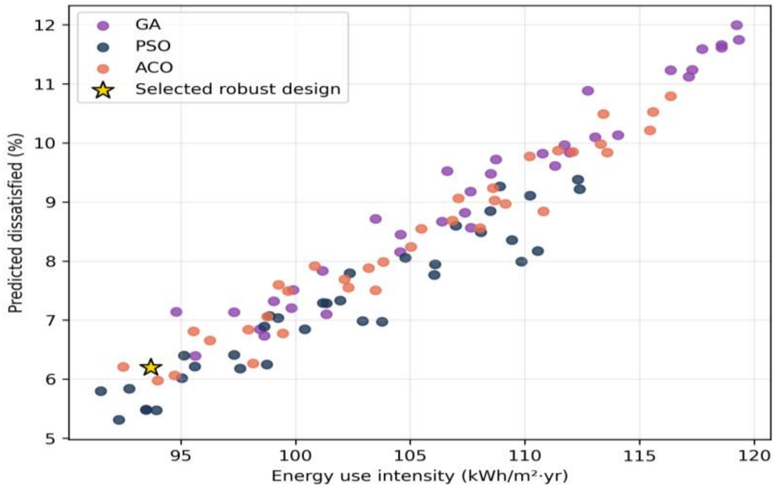


Figure 4. Pareto-optimal solutions from GA, PSO, and ACO

### 2.8. Decision-analysis calculations

#### 2.8.1. Entropy weighting

For *m* alternatives and n criteria, the normalized decision matrix is:

$$r_{ij} = \frac{x_{ij}}{\sqrt{\sum_{i=1}^{m} x_{ij}^2}}. \tag{29}$$

The entropy probability and entropy value are:

$$p_{ij} = \frac{r_{ij}}{\sum_{i=1}^{m} r_{ij}}, \qquad e_j = -\frac{1}{\ln(m)}\sum_{i=1}^{m} p_{ij}\ln\left(p_{ij}\right). \tag{30}$$

The entropy weight is:

$$w_j = \frac{1-e_j}{\sum_{j=1}^{n}(1-e_j)}. \tag{31}$$

Table 3 below expresses the entropy, divergence, and weight values for the major criteria under this model.

Table 3. Decision variables and numerical bounds

| Criterion | Entropy $e_j$ | Divergence $1-e_j$ | Weight $w_j$ |
|---|---|---|---|
| EUI | 0.914 | 0.086 | 0.223 |
| Discomfort hours | 0.887 | 0.113 | 0.293 |
| Carbon intensity | 0.925 | 0.075 | 0.194 |
| UDI | 0.948 | 0.052 | 0.135 |
| RT60 | 0.940 | 0.060 | 0.155 |
| Total | - | 0.386 | 1.000 |

### 2.8.2. TOPSIS ranking

The weighted normalized matrix is:

$$v_{ij} = w_j r_{ij}. \quad (32)$$

The positive and negative ideal distances are:

$$D_i^+ = \sqrt{\sum_{j=1}^{n}\left(v_{ij} - v_j^+\right)^2}, \qquad D_i^- = \sqrt{\sum_{j=1}^{n}\left(v_{ij} - v_j^-\right)^2}. \quad (33)$$

The TOPSIS closeness coefficient is:

$$CC_i = \frac{D_i^-}{D_i^+ + D_i^-}. \quad (34)$$

For the PSO solution, using $D^+$*=0.041* and $D^-$*=0.219*:

$$CC_{PSO} = \frac{0.219}{0.041+0.219} = 0.842. \quad (35)$$

Table 4 summarizes the TOPSIS ranking of the three bioinspired alternatives.

Table 4. TOPSIS ranking of bioinspired alternatives

| Alternative | $D^+$ | $D^-$ | $CC_i$ | Rank |
|---|---|---|---|---|
| GA | 0.083 | 0.166 | 0.667 | 3 |
| PSO | 0.041 | 0.219 | 0.842 | 1 |
| ACO | 0.064 | 0.191 | 0.749 | 2 |

### 2.8.3. Composite pedagogic sustainability index

The composite index is:

$$PSI_i = \sum_{j=1}^{n} w_j\, r_{ij}. \quad (36)$$

The numerical PSI values are:

$$PSI_{GA} = 0.781, \qquad PSI_{PSO} = 0.835, \qquad PSI_{ACO} = 0.804. \quad (37)$$

F The relative gain of PSO over GA is:

$$G_{PSO/GA} = \frac{0.835-0.781}{0.781} \times 100 = 6.91\%. \quad (38)$$

Figure 5 reports the global sensitivity indices for the pedagogic sustainability index.

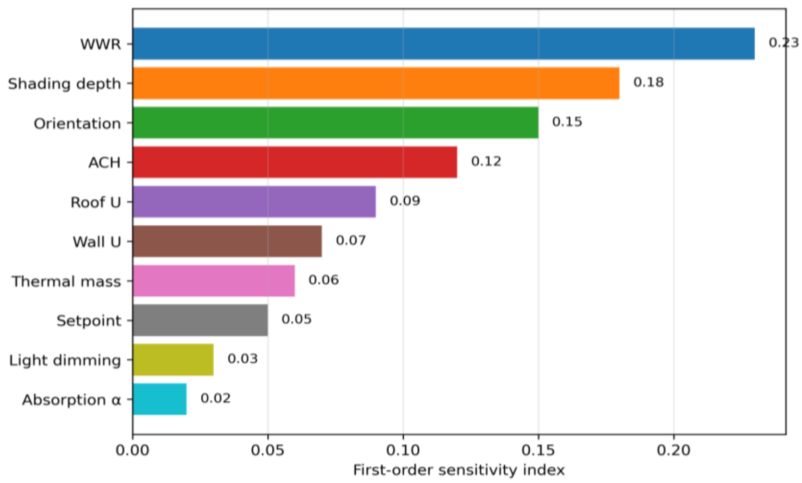


Figure 5. Global sensitivity of the pedagogic sustainability index

## 3. Results and discussion

### 3.1. Energy and carbon results

The optimized end-use distribution is shown in Figure 6. Cooling is the dominant contributor to improvement because optimized shading, glazing, insulation, and setpoint decisions act together. Lighting also reduces because daylight dimming is coordinated with the window-to-wall ratio.

Figure 6 presents the optimized end-use distribution before and after the robust design improvement.

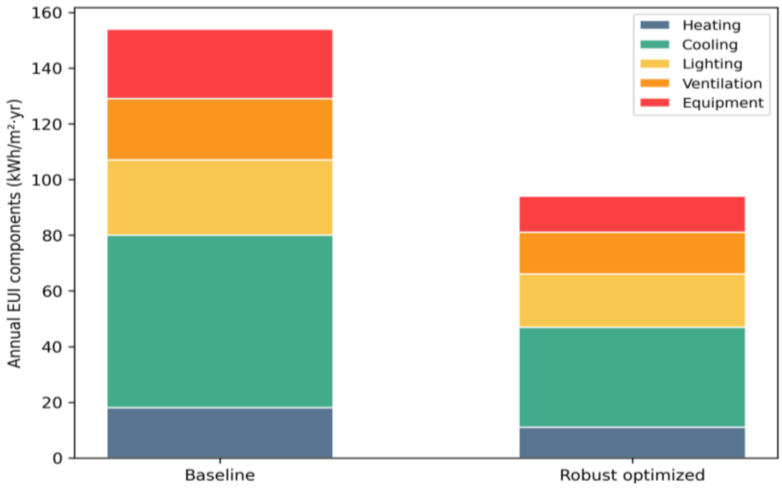


Figure 6. End-use decomposition before and after optimization

Table 5 compares the baseline and optimized performance outcomes for the main design indicators.

Table 5. TOPSIS ranking of bioinspired alternatives

| Metric | Baseline | GA | PSO | ACO | Best improvement |
|---|---|---|---|---|---|
| EUI (kWh/m²·yr) | 154.2 | 101.8 | 93.7 | 98.9 | 39.2% |
| Carbon (kgCO2e/m²·yr) | 127.8 | 82.9 | 75.4 | 79.3 | 41.0% |
| Discomfort hours (h/yr) | 418 | 201 | 143 | 177 | 65.8% |
| UDI (%) | 54.8 | 76.9 | 81.2 | 78.5 | 48.2% |
| STI | 0.56 | 0.66 | 0.71 | 0.68 | 26.8% |
| RT60 (s) | 0.92 | 0.64 | 0.59 | 0.62 | 35.9% |
| CO2 (ppm) | 1128 | 866 | 794 | 832 | 29.6% |
| PSI | 0.412 | 0.781 | 0.835 | 0.804 | 102.7% |

### 3.2. Algorithmic performance statistics

Hypervolume is computed as:

$$HV(S) = \lambda\left(\bigcup_{\mathbf{y}\in S}[y_1, r_1] \times [y_2, r_2] \times \cdots \times [y_d, r_d]\right). \tag{39}$$

The generational distance plus statistic is:

$$GD^{+} = \frac{1}{|S|}\left(\sum_{\mathbf{s}\in S} d^{+}(\mathbf{s}, PF)^2\right)^{1/2}. \tag{40}$$

Spacing is:

$$SP = \sqrt{\frac{1}{|S|-1}\sum_{i=1}^{|S|}\left(\bar{d} - d_i\right)^2}. \tag{41}$$

Table 6 reports the algorithmic comparison across ten random seeds.

Table 6. Algorithmic comparison over ten random seeds

| Algorithm | Hypervolume | GD+ | Spacing | Runtime (min) | Selected PSI |
|---|---|---|---|---|---|
| GA | 0.841 ± 0.010 | 0.042 ± 0.006 | 0.073 ± 0.011 | 47.6 ± 2.5 | 0.781 ± 0.012 |
| PSO | 0.872 ± 0.006 | 0.027 ± 0.004 | 0.061 ± 0.008 | 39.4 ± 2.1 | 0.835 ± 0.009 |
| ACO | 0.856 ± 0.008 | 0.034 ± 0.005 | 0.068 ± 0.010 | 44.8 ± 2.7 | 0.804 ± 0.010 |

### 3.3. Alpha-cut uncertainty propagation

Let $\tilde{x}$ be a triangular fuzzy variable with lower, modal, and upper values *(a,b,c)*. Its $\alpha$-cut is:

$$\tilde{x}_\alpha = [a + \alpha(b - a),\ c - \alpha(c - b)]. \tag{42}$$

For EUI represented as *(88.4,93.7,103.1)*, the $\alpha$*=0.6* interval is:

$$EUI_{0.6} = [88.4 + 0.6(93.7 - 88.4),\ 103.1 - 0.6(103.1 - 93.7)] = [91.58,97.46]. \tag{43}$$

For carbon intensity represented as *(70.2,75.4,82.8)*, the $\alpha$*=0.6* interval is:

$$CI_{0.6} = [70.2 + 0.6(75.4 - 70.2),\ 82.8 - 0.6(82.8 - 75.4)] = [73.32,78.36]. \tag{44}$$

Table 7 presents alpha-cut intervals for the selected PSO design.

Table 7. Alpha-cut intervals for selected PSO design

| **α** | **EUI interval** | **Carbon interval** | **PPD interval** | **UDI interval** |
|---|---|---|---|---|
| 0.0 | [88.40, 103.10] | [70.20, 82.80] | [5.40, 9.80] | [75.60, 84.70] |
| 0.2 | [89.46, 101.22] | [71.24, 81.32] | [5.76, 9.28] | [76.72, 84.00] |
| 0.4 | [90.52, 99.34] | [72.28, 79.84] | [6.12, 8.76] | [77.84, 83.30] |
| 0.6 | [91.58, 97.46] | [73.32, 78.36] | [6.48, 8.24] | [78.96, 82.60] |
| 0.8 | [92.64, 95.58] | [74.36, 76.88] | [6.84, 7.72] | [80.08, 81.90] |
| 1.0 | [93.70, 93.70] | [75.40, 75.40] | [7.20, 7.20] | [81.20, 81.20] |

Figure 7 illustrates the Monte Carlo robustness distribution of the selected PSO-based design.

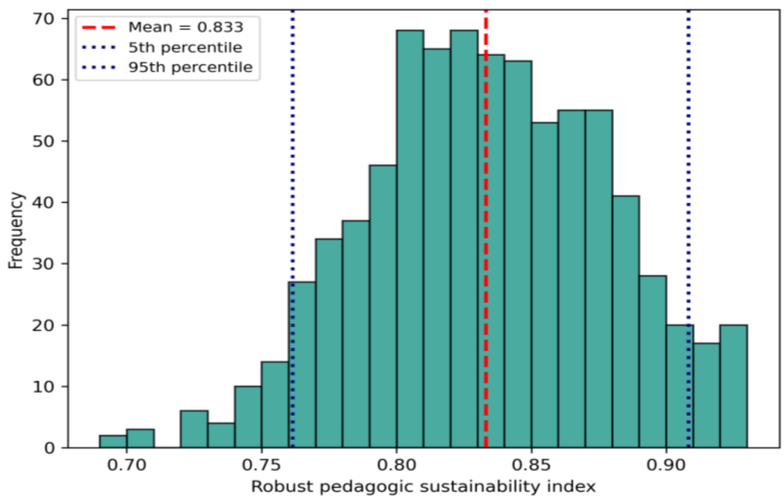


Figure 7. Monte Carlo robustness distribution of the selected design

### 3.4. Reliability formulation

Let $R_j$ be the reliability of performance indicator j. Assuming a Weibull-type reliability model:

$$R_j(t) = \exp\left[-\left(\frac{t}{\eta_j}\right)^{\beta_j}\right]. \tag{45}$$

A weighted building-performance reliability score is:

$$R_B = \prod_{j=1}^{n} R_j^{w_j}. \tag{46}$$

Using $R_{EUI}=0.93$, $R_{CO2}=0.91$, $R_{PMV}=0.89$, $R_{UDI}=0.92$, and $R_{RT}=0.90$, the resulting score is:

$$R_B = 0.93^{0.223} \times 0.91^{0.194} \times 0.89^{0.293} \times 0.92^{0.135} \times 0.90^{0.155} = 0.910. \tag{47}$$

### 3.5. Adaptive control results

The interval type-2 fuzzy controller uses occupancy, carbon dioxide, daylight, outdoor temperature, and thermal error as inputs.

The firing interval of rule *r* is:

$$\underline{w}_r = \prod_{q=1}^{Q} \underline{\mu}_{A_{rq}}(z_q), \qquad \overline{w}_r = \prod_{q=1}^{Q} \overline{\mu}_{A_{rq}}(z_q). \tag{48}$$

The type-reduced control output is approximated as:

$$u(t) = \frac{\sum_{r=1}^{R} \bar{w}_r y_r}{\sum_{r=1}^{R} \bar{w}_r}, \qquad \bar{w}_r = \frac{\underline{w}_r + \overline{w}_r}{2}. \tag{49}$$

The daily operational saving is:

$$S_{day} = \frac{669-551}{669} \times 100 = 17.6\%. \tag{50}$$

Figure 8 shows the adaptive-control response under dynamic classroom occupancy and compares rule-based and adaptive energy behavior.

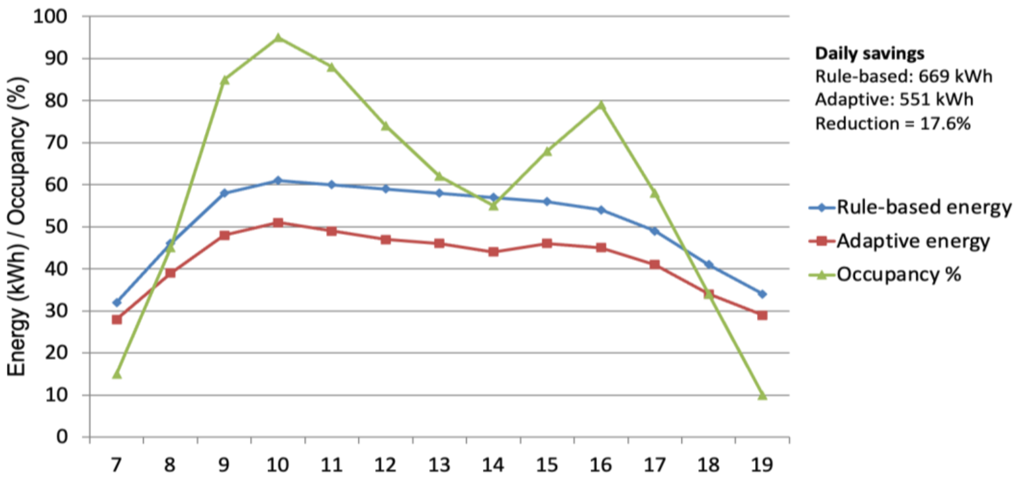


Figure 8. Adaptive control response under dynamic classroom occupancy

Table 8 compares the adaptive-control numerical scenarios.

Table 8. Alpha-cut intervals for selected PSO design

| Scenario | Daily energy (kWh) | Mean CO2 (ppm) | Discomfort hours (%) | Lighting adequacy (%) |
|---|---|---|---|---|
| S1 fixed rule-based | 669 | 1008 | 9.7 | 86.1 |
| S2 ventilation-adaptive | 621 | 902 | 8.1 | 86.4 |

| Scenario | Daily energy (kWh) | Mean CO2 (ppm) | Discomfort hours (%) | Lighting adequacy (%) |
|---|---|---|---|---|
| S3 HVAC + lighting adaptive | 583 | 832 | 6.6 | 90.5 |
| S4 full IT2 fuzzy adaptive | 551 | 792 | 5.8 | 92.3 |

## 3.6. Additional numerical verification

### 3.6.1. Worked calculation of weighted normalized scores

The benefit-normalized value is:

$$r_{ij}^{B}=\frac{x_{ij}-x_j^{min}}{x_j^{max}-x_j^{min}}. \tag{51}$$

The cost-normalized value is:

$$r_{ij}^{C}=\frac{x_j^{max}-x_{ij}}{x_j^{max}-x_j^{min}}. \tag{52}$$

For EUI, with $x^{max}$=154.2 and $x^{min}$=93.7, the PSO-normalized cost score is:

$$r_{PSO,EUI}^{C}=\frac{154.2-93.7}{154.2-93.7}=1.000. \tag{53}$$

For UDI, using $x^{max}=81.2$ and $x^{min}=54.8$, the PSO benefit score is:

$$r_{PSO,UDI}^{B}=\frac{81.2-54.8}{81.2-54.8}=1.000. \tag{54}$$

For GA on EUI:

$$r_{GA,EUI}^{C}=\frac{154.2-101.8}{154.2-93.7}=0.866. \tag{55}$$

Figure 9 summarizes the entropy-TOPSIS scoring procedure and the final ranking of baseline, GA, PSO, and ACO alternatives.

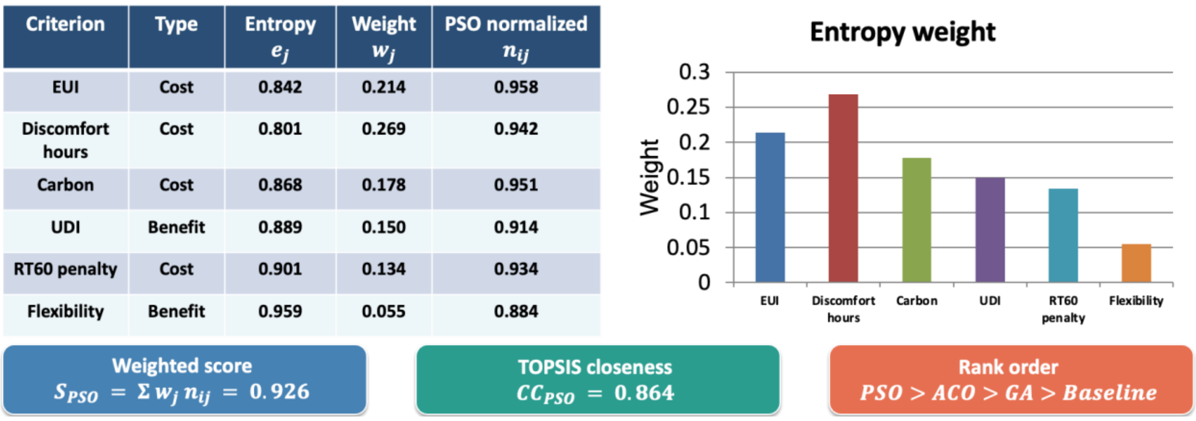

| Criterion | Type | Entropy $e_j$ | Weight $w_j$ | PSO normalized $n_{ij}$ |
|---|---|---|---|---|
| EUI | Cost | 0.842 | 0.214 | 0.958 |
| Discomfort hours | Cost | 0.801 | 0.269 | 0.942 |
| Carbon | Cost | 0.868 | 0.178 | 0.951 |
| UDI | Benefit | 0.889 | 0.150 | 0.914 |
| RT60 penalty | Cost | 0.901 | 0.134 | 0.934 |
| Flexibility | Benefit | 0.959 | 0.055 | 0.884 |



Figure 9. Entropy-TOPSIS score comparison for baseline, GA, PSO, and ACO solutions

### 3.6.2. Scenario matrix for timetable uncertainty

The uncertainty multiplier for occupancy scenario $s$ is:

$$\kappa_s=1+\Delta_o^s+\Delta_w^s+\Delta_g^s. \tag{56}$$

The cost-normalized value is:

$$EUI_s=EUI_o\kappa_s. \tag{57}$$

For a high-occupancy hot-day scenario with $\Delta_o=0.08$, $\Delta_w=0.06$, and $\Delta_g=0.03$,

$$EUI_s = 93.7(1 + 0.08 + 0.06 + 0.03) = 109.63 \text{ kWh/m}^2\text{yr}. \tag{58}$$

Table 9 summarizes the timetable and weather-scenario calculations.

Table 9. Timetable and weather scenario calculations

| Scenario | Occupancy change | Weather change | Gain change | $\kappa_s$ | Adjusted EUI |
|---|---|---|---|---|---|
| Low-use examination period | -0.12 | -0.02 | -0.04 | 0.82 | 76.83 |
| Normal semester | 0.00 | 0.00 | 0.00 | 1.00 | 93.70 |
| Hot high-occupancy week | 0.08 | 0.06 | 0.03 | 1.17 | 109.63 |
| Hybrid low-occupancy week | -0.18 | 0.02 | -0.01 | 0.83 | 77.77 |

Figure 10 presents the alpha-cut uncertainty envelope and reliability calculation for the selected PSO design.

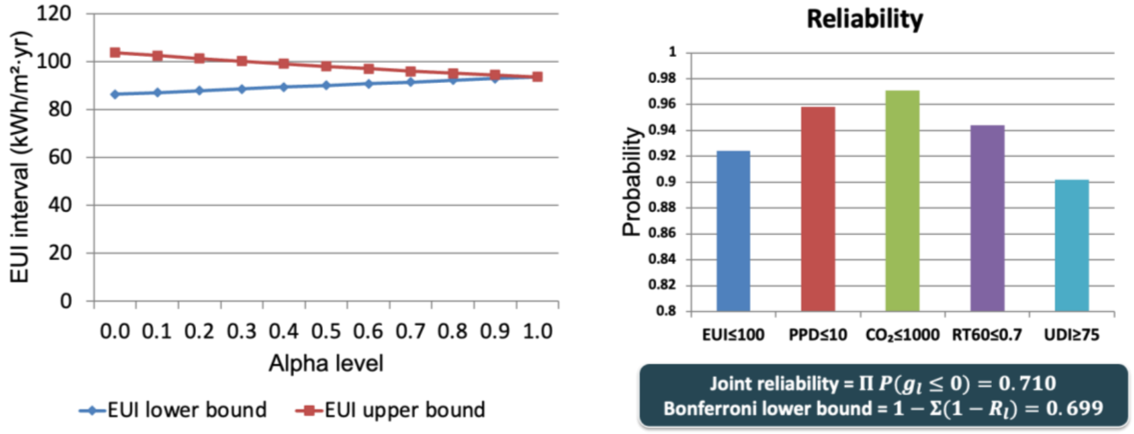


Figure 10. Alpha-cut uncertainty envelope and reliability calculation for the selected PSO design

### 3.6.3. Reliability-based robust score and worked dashboard interpretation

Let $r_i=[r_{i1},r_{i2},\dots,r_{in}]$ be the normalized performance vector. A balanced-design penalty is defined as:

$$B_i = 1 - \sqrt{\frac{1}{n}\sum_{j=1}^{n}\left(r_{ij} - \bar{r}_i\right)^2}. \tag{59}$$

The final robust score combines the sustainability index, reliability, and balance:

$$RS_i = 0.60PSI_i + 0.25R_i + 0.15B_i. \tag{60}$$

For the PSO design, using $PSI=0.835$, $R=0.910$, and $B=0.884$:

$$RS_{PSO} = 0.60(0.835) + 0.25(0.910) + 0.15(0.884) = 0.861. \tag{61}$$

Figure 11 provides a worked numerical dashboard for energy, carbon, and adaptive-control savings.

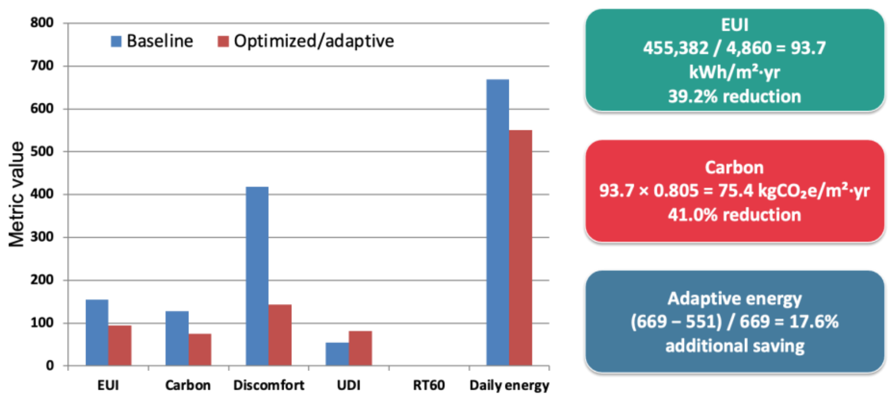


Figure 11. Worked on a numerical calculation dashboard for energy, carbon, and adaptive control savings

Three typical numerical computations, i.e., annual EUI cutback (J), optimized carbon-intensity conversion (kgCO2/kWh), and daily power-saving from adaptive fuzzy control (%), are consolidated in Fig. 11(a), along with values that all comply with the calendar year monthly distribution depicted by Fig.11(b). This computation also allows engineering readers and institutional decision-makers to interpret performance more easily.

### 3.6.4. Engineering-scale energy-saving and carbon-abatement verification

The engineering-scale verification translates normalized performance indicators into annual building quantities. This step is necessary because EUI and carbon intensity are convenient comparison metrics, but institutional planners need annual energy demand, annual carbon reduction, and controller-level savings in absolute units.

Let the gross floor area of the representative learning center be defined as:

$A_f=4,860\ m^2$.

Using the baseline EUI of 154.2 kWh/m²·year, the baseline annual energy demand is calculated as:

$E_{base}=EUI_{base}\times A_f=154.2\times 4,860=749,412\ kWh/year$.

For the selected PSO-based optimized design, the annual energy demand becomes:

$E_{PSO}=EUI_{PSO}\times A_f=93.7\times 4,860=455,382\ kWh/year$.

Therefore, the design-stage annual energy saving is:

$\Delta E_{design}=E_{base}–E_{PSO}=749,412–455,382=294,030\ kWh/year$.

The corresponding design-stage energy-saving percentage is:

Energy saving percentage = (294,030 / 749,412) × 100 = 39.24%.

Similarly, annual carbon emission is obtained by multiplying the carbon intensity by the same gross floor area. For the baseline case:

$C_{base}=127.8\times 4,860=621,108\ kgCO_2e/year=621.108\ tCO_2e/year$.

For the optimized PSO design:

$C_{PSO}=75.4\times 4,860=366,444\ kgCO_2e/year=366.444\ tCO_2e/year$.

The annual carbon-abatement value is therefore:

$\Delta C=C_{base}–C_{PSO}=621,108–366,444=254,664\ kgCO_2e/year=254.664\ tCO_2e/year$.

The corresponding carbon-reduction percentage is: *(254,664 / 621,108) × 100 = 41.00%.*

The operation-stage contribution was verified using the daily control scenarios. The fixed rule-based operation and full interval type-2 fuzzy adaptive-control operation are represented as:

$E_F=669;\ EIT2=551\ kWh/day$.

Thus, the daily adaptive-control saving is:

$\Delta Eday=EF–EIT2=669–551=118\ kWh/day$.

The daily adaptive-control saving percentage is: *(118 / 669) × 100 = 17.64%.*

If the learning center operates under active academic conditions for 250 teaching and working days in a year, the annual adaptive-control saving is:

$\Delta E_{year}=\Delta E_{day}\times N_{op}=118\times 250=29,500\ kWh/year$.

These computations verify two levels of architectural and environmental co-benefit. First, annual energy use and carbon emissions are reduced at the building-design level. Second, the adaptive controller provides operational-stage savings that can be measured while allowing the learning center to function as a responsive architectural system rather than a fixed engineering object. Using the same equations as in this section, Table 10 confirms the annual energy savings, carbon reduction, and adaptive-control benefits at an engineering and architectural scale.

Table 10. Engineering-scale verification of annual performance improvement

| Indicator | Calculation | Numerical result |
|---|---|---|
| Baseline annual energy | *154.2×4,860* | 749,412 kWh/year |
| Optimized annual energy | *93.7×4,860* | 455,382 kWh/year |
| Annual energy saving | *749,412-455,382* | 294,030 kWh/year |
| Energy saving percentage | *294,030/749,412×100* | 39.24% |
| Baseline annual carbon | *127.8×4,860* | 621,108 kgCO2e/year |
| Optimized annual carbon | *75.4×4,860* | 366,444 kgCO2e/year |
| Annual carbon reduction | *621,108-366,444* | 254,664 kgCO2e/year |
| Annual carbon reduction in tonnes | *254,664/1,000* | 254.664 tCO2e/year |
| Carbon reduction percentage | *254,664/621,108×100* | 41.00% |
| Daily adaptive-control saving | *669-551* | 118 kWh/day |
| Daily adaptive saving percentage | *118/669×100* | 17.64% |
| Annual adaptive-control saving | *118×250* | 29,500 kWh/year |

### 3.7. Discussion

The discussion is organized by the four research objectives presented in the introduction. To address objective (i), the proposed work presents a mathematically transparent framework within which thermal balance, carbon dioxide balance, daylight adequacy, reverberation, plus graph-based spatial flexibility and surrogate error entropy weighting are interpreted as architectural performance quantities, thus the TOPSIS closeness. In this sense, the proposed mathematical framework addresses the architectural problem by relating measurable metrics with room proportion, facade design, circulation mode, space flexibility, as well as user comfort.

For objective (ii), based on the performance of GA, PSO, and ACO studied in this work for the same numerical budget, we found that out of this design space and with no parameter fine-tuning for the searching method, PSO provided better overall results. In addition to the forum score of the top frequently reviewed solution, it also presents the hypervolume, GD+ value, spacing, and execution time with selected PSI for the PSO solution compared to different test algorithms. This does not mean that PSO is universally superior; rather, for this educational-building typology, PSO better fitted the continuous envelope, comfort, daylight, acoustic, and adaptive-control variables.

As for objective (iii), the gains achieved at both normalized and building scales are considerable as compared to the conventional design. The optimal design (PSO) decreased the EUI from 154.2 to 93.7 kWh/m²·year, carbon intensity from 127.8 to 75.4 kgCO2e/m²·year [30], discomfort hours from 418 to 143 h/year, and RT60 [24]. At the engineering scale, they are equivalent to an energy saving of 2730 MWh/yr and a carbon reduction of 254734 tCO2e/yér respectively. In the daily scenario, the interval type-2 fuzzy adaptive-control layer contributes to deeper energy savings of 118 kWh/day, amounting to 29,500 kWh/year over 250 active academic operating days.

For objective (iii), the gains achieved at both normalized and building scales are considerable when compared with the conventional design [47]. The optimized PSO design reduced EUI from 154.2 to 93.7 kWh/m²·year, carbon intensity from 127.8 to 75.4 kgCO2e/m²·year, discomfort hours from 418 to 143 h/year, and RT60 from 0.92 to 0.59 s. At the engineering scale, these values correspond to an annual energy saving of 294.030 MWh/year and an annual carbon reduction of 254.664 tCO2e/year. In the daily scenario, the interval type-2 fuzzy adaptive-control layer contributes an additional saving of 118 kWh/day, amounting to 29,500 kWh/year over 250 active academic operating days.

For objective (iv), the fuzzy-bioinspired framework we propose provides two relevant approach-oriented benefits. In the first, bioinspired optimization seeks out design choices to balance energy, carbon, thermal comfort, daylight and acoustic performance but also spatial adaptability. Second, controlled occupancy and lighting scenario with uncertainty in position is represented via interval type-2 fuzzy rules to interpret operating rules under uncertain carbon dioxide and thermal-error scenarios. These matters, too, to educational institutions because facility managers can track how the adaptive system supports real users in real spaces rather than rely exclusively on opaque numerical outputs.

The findings from PSO point to a small but penetrable learning-center design that incorporates lower moderate proportional glazing, increased external shading depth, improved roof and wall insulation values, greater acoustic absorption capacity, and corridors which are open enough for supervision / social learning while still providing acoustic comfort in teaching spaces. The results also imply that sustainable educational architecture should be evaluated through user pathways, flexible room typologies, daylight distribution, and post-occupancy adaptability, not only through energy and carbon metrics.

Comparison with other similar research also clarifies the novelty of the present research. Proot-Lafontaine et al. focused solely on indoor environmental quality in a school building. In contrast, this study integrates IEQ with energy, carbon, spatial flexibility, robustness, and adaptive control into a single optimization framework [48].

Miri et al. considered how the quality of the indoor environment influences students' attention and relaxation during lecture-based instruction, whereas the present study translates those environmental concerns into optimization objectives and performance constraints [49, 50]. Building on Brink et al. [51], who demonstrated the importance of indoor environmental conditions for higher-education classroom performance, the present framework provides a computational approach for selecting and operating design alternatives before full-scale implementation. Energy efficiency, one of the most effective means of minimizing energy demand, is emphasized by the International Energy Agency (IEA) [52], and this study's numerical results illustrate its ground-level operationalization in integrated design and control at the educational-building scale.

The study remains simulation-based. Calibrated sensors should be validated with real class schedules, measured plug-load profiles, and post-occupancy evaluations for future validation. But the framework is still a valuable blueprint, as every indicator has some physical or decision-analytic interpretation, which designers and facility managers can apply. So more than energy efficiency, the main contribution is an architectural decision pathway to design user-centered learning environments that are spatially flexible and resilient to variability in timetables, weather, and occupancy.

## 4. Conclusions

This study gives a mathematically sound and architecturally interpreted basis for digital and bioinspired methodologies. Sustainable educational environments: modeling, optimizations, and adaptive reaction mechanisms. It presents a BIM-linked co-simulation framework supported by surrogate modeling, GA, PSO, ACO, entropy weighting, TOPSIS ranking, alpha-cut uncertainty propagation, reliability scoring, and interval type-2 fuzzy adaptive control, while translating these computational layers into spatial typology, user comfort, adaptive pedagogy, and architectural design implications. A robust PSO design achieved lower EUI (reduced from 154.2 to 93.7 kWh/m²·yr), carbon (from 127.8 to 75.4 kgCO2e/m²·yr), discomfort hours (from 418 to 143 h/year) and RT60 (from 0.92 to 0.59 s), and higher UDI (54.8%–81.2%) and pedagogic sustainability index (0.412-0.835).

The complete adaptive-control case further reduced daily energy use from 669 to 551 kWh/day. These numerical results support the main conclusion that sustainable educational spaces should function as adaptive, bioinspired systems rather than static architectural vessels. The architectural conclusion is that sustainable educational spaces should be planned as adaptable typological systems in which facade depth, classroom clustering, circulation openness, acoustic buffering, daylight control, and user-responsive operation are considered together from the early design stage. Future work should combine embodied carbon, life-cycle cost, measured campus data, real occupancy sensors, and agent-based movement models. Further research might also link AR/VR learning needs more directly with lighting, acoustic and thermal comfort limits.

### Declaration of competing interests

The authors declare that they have no known financial or non-financial competing interests in any material discussed in this paper.

### Funding information

No funding was received from any financial organization to conduct this research.

### Author contribution

The contribution to the paper is as follows: A. Anafina, A. Kornilova: study conception and design; A. Anafina: data collection; A. Anafina, A. Kornilova: analysis and interpretation of results; A. Kornilova: draft preparation. All authors approved the final version of the manuscript.

### References

[1] *United Nations, The Sustainable Development Goals Report 2024*. New York, NY, USA: United Nations, 2024.

[2] L. Mykhailova, O. Kozak, and H. Chyrva, "Augmented Educational Reality: Integrating AR Technologies into the Future Learning Process", *Futurity Education*, vol. 4, no. 1, pp. 71-85, 2024. https://doi.org/10.57125/FED.2024.03.25.04

[3] O. Prokopenko and A. Sapinski, "Using Virtual Reality in Education: Ethical and Social Dimensions", *E-Learning Innovations Journal*, vol. 2, no. 1, pp. 41-62, 2024. https://doi.org/10.57125/ELIJ.2024.03.25.03

[4] E. Kamel and A. M. Memari, "Review of BIM's application in energy simulation: Tools, issues, and solutions", *Automation in Construction*, vol. 97, pp. 164-180, 2019. https://doi.org/10.1016/j.autcon.2018.11.008

[5] H. S. P. C. Garcez, P. J. da Silva, and R. A. M. Rodrigues, "BIM-based sustainability assessment: An analysis of interoperability challenges", *Journal of Cleaner Production*, vol. 256, Art. 120419, 2020. https://doi.org/10.1016/j.jclepro.2020.120419

[6] M. Parn, D. J. Edwards, and M. C. P. Sing, "The building information modelling trajectory in facilities management: A review", *Automation in Construction*, vol. 75, pp. 45-55, 2017. https://doi.org/10.1016/j.autcon.2016.12.003

[7] X. Li and J. Wen, "Review of building energy modeling for control and operation", *Renewable and Sustainable Energy Reviews*, vol. 37, pp. 517-537, 2014. https://doi.org/10.1016/j.rser.2014.05.056

[8] A.-T. Nguyen, S. Reiter, and P. Rigo, "A review on simulation-based optimization methods applied to building performance analysis", *Applied Energy*, vol. 113, pp. 1043-1058, 2014. https://doi.org/10.1016/j.apenergy.2013.08.061

[9] F. Kheiri, "A review on optimization methods applied in energy-efficient building geometry and envelope design", *Renewable and Sustainable Energy Reviews*, vol. 92, pp. 897-920, 2018. https://doi.org/10.1016/j.rser.2018.04.080

[10] L. Zhang, R. P. Pang, A. H. E. Hassani, and A. T. S. Chan, "Optimization of the daylighting and energy performance of school buildings based on parametric algorithm", *Energy and Buildings*, vol. 244, Art. 111033, 2021. https://doi.org/10.1016/j.enbuild.2021.111033

[11] Y. Ji, Y. Zhang, Y. Han, and X. Luo, "Performance in generation: An automatic generalizable generative-design-based performance optimization framework for sustainable building design", *Energy and Buildings*, vol. 298, Art. 113512, 2023. https://doi.org/10.1016/j.enbuild.2023.113512

[12] C. E. Madubuike, C. O. Anumba, and R. Khallaf, "A review of digital twin applications in construction", *Journal of Information Technology in Construction*, vol. 27, pp. 145-172, 2022. https://doi.org/10.36680/j.itcon.2022.008

[13] H. Omrany, S. A. H. Shah, et al., "Digital twins in the construction industry: A comprehensive review of current implementations and future directions", *Sustainability*, vol. 15, no. 14, Art. 10908, 2023. https://doi.org/10.3390/su151410908

[14] L. C. Tagliabue, F. Cecconi, A. Rinaldi, and M. Ciribini, "Leveraging digital twin for sustainability assessment of an existing building", *Sustainability*, vol. 13, no. 2, Art. 480, 2021. https://doi.org/10.3390/su13020480

[15] K. Backlund, J. Johansson, and L. K. Maas, "Showcasing a digital twin for higher educational buildings: Developing the concept toward human centricity", *Frontiers in Built Environment*, vol. 10, Art. 1347451, 2024. https://doi.org/10.3389/fbuil.2024.1347451

[16] N. Delgarm, B. Sajadi, F. Kowsary, and S. Delgarm, "Multi-objective optimization of the building energy performance: A simulation-based approach by means of particle swarm optimization", *Applied Energy*, vol. 170, pp. 293-303, 2016. https://doi.org/10.1016/j.apenergy.2016.02.141

[17] N. Delgarm, B. Sajadi, and S. Delgarm, "Multi-objective optimization of building energy performance and indoor thermal comfort: A new method using artificial bee colony", *Energy and Buildings*, vol. 131, pp. 42-53, 2016. https://doi.org/10.1016/j.enbuild.2016.09.003

[18] M. Hamdy, A.-T. Nguyen, and J. L. M. Hensen, "A performance comparison of multi-objective optimization algorithms for solving nearly-zero-energy-building design problems", *Energy and Buildings*, vol. 121, pp. 57-71, 2016. https://doi.org/10.1016/j.enbuild.2016.03.035

[19] D. Tuhus-Dubrow and M. Krarti, "Genetic-algorithm based approach to optimize building envelope design for residential buildings", *Building and Environment*, vol. 45, no. 7, pp. 1574-1581, 2010. https://doi.org/10.1016/j.buildenv.2010.01.005

[20] A. Ciardiello, F. Rosso, J. Dell'Olmo, V. Ciancio, M. Ferrero, and F. Salata, "Multi-objective approach to the optimization of shape and envelope in building energy design", *Applied Energy*, vol. 280, Art. 115984, 2020. https://doi.org/10.1016/j.apenergy.2020.115984

[21] T. Mendez Echenagucia, A. Capozzoli, Y. Cascone, and M. Sassone, "The early design stage of a building envelope: Multi-objective search through heating, cooling and lighting energy performance analysis", *Applied Energy*, vol. 154, pp. 577-591, 2015. https://doi.org/10.1016/j.apenergy.2015.04.090

[22] F. Carlucci, F. Causone, L. De Rosa, and F. Pagliano, "Multi-objective optimization of a nearly zero-energy building based on thermal and visual discomfort minimization using NSGA-II", *Energy and Buildings*, vol. 104, pp. 378-394, 2015. https://doi.org/10.1016/j.enbuild.2015.06.064

[23] H. Y. Huang, L. C. Lin, M. T. Ke, T. Sathesh, and W. S. Lee, "Energy performance evaluation for benchmarking school buildings using dynamic clustering analysis and particle swarm optimization", *Building Services Engineering Research and Technology*, vol. 41, no. 4, pp. 429-440, 2020. https://doi.org/10.1177/0143624419879001

[24] R. J. Shaughnessy, U. Haverinen-Shaughnessy, A. Nevalainen, and D. Moschandreas, "A preliminary study on the association between ventilation rates in classrooms and student performance", *Indoor Air*, vol. 16, no. 6, pp. 465-468, 2006. https://doi.org/10.1111/j.1600-0668.2006.00440.x

[25] M. Turunen, O. Toyinbo, T. Putus, A. Nevalainen, R. Shaughnessy, and U. Haverinen-Shaughnessy, "Indoor environmental quality in school buildings, and the health and wellbeing of students", *International Journal of Hygiene and Environmental Health*, vol. 217, no. 7, pp. 733-739, 2014. https://doi.org/10.1016/j.ijheh.2014.03.002

[26] H. W. Brink, M. G. L. C. Loomans, M. P. Mobach, and H. S. M. Kort, "Classrooms' indoor environmental conditions affecting the academic achievement of students and teachers in higher education: A systematic literature review", *Indoor Air*, vol. 31, no. 2, pp. 405-425, 2021. https://doi.org/10.1111/ina.12745

[27] M. C. Lee, K. W. Mui, L. T. Wong, W. Y. Chan, E. W. M. Lee, and C. T. Cheung, "Student learning performance and indoor environmental quality in air-conditioned university teaching rooms", *Building and Environment*, vol. 49, pp. 238-244, 2012. https://doi.org/10.1016/j.buildenv.2011.10.001

[28] P. Barrett, F. Davies, Y. Zhang, and L. Barrett, "The impact of classroom design on pupils' learning: Final results of a holistic, multi-level analysis", *Building and Environment*, vol. 89, pp. 118-133, 2015. https://doi.org/10.1016/j.buildenv.2015.02.013

[29] J. Palacios Temprano, P. Eichholtz, M. Willeboordse, and N. Kok, "Indoor environmental quality and learning outcomes: Protocol on large-scale sensor deployment in schools", *BMJ Open*, vol. 10, no. 3, e031233, 2020. https://doi.org/10.1136/bmjopen-2019-031233

[30] H. B. Gunay, W. O'Brien, I. Beausoleil-Morrison, and S. Gilani, "Development and implementation of an adaptive lighting and blinds control algorithm", *Building and Environment*, vol. 113, pp. 185-199, 2017. https://doi.org/10.1016/j.buildenv.2016.08.027

[31] D. Caicedo and A. Pandharipande, "Daylight and occupancy adaptive lighting control system: An iterative optimization approach", *Lighting Research & Technology*, vol. 48, no. 6, pp. 661-675, 2016. https://doi.org/10.1177/1477153515587148

[32] M. Killian and M. Kozek, "Ten questions concerning model predictive control for energy efficient buildings", *Building and Environment*, vol. 105, pp. 403-412, 2016. https://doi.org/10.1016/j.buildenv.2016.05.034

[33] F. Hou, J. C. P. Cheng, J. Ma, H. H. L. Kwok, C. Huang, and Z. Wu, "Occupancy-driven HVAC control optimization via LSTM and deep reinforcement learning for enhanced indoor air quality, thermal comfort and energy efficiency", *Building and Environment*, vol. 284, Art. 113501, 2025. https://doi.org/10.1016/j.buildenv.2025.113501

[34] L. M. Escobar, J. Aguilar, A. Garces-Jimenez, J. A. Gutierrez De Mesa, and J. M. Gomez-Pulido, "Advanced fuzzy-logic-based context-driven control for HVAC management systems in buildings", *IEEE Access*, vol. 8, pp. 16111-16126, 2020. https://doi.org/10.1109/ACCESS.2020.2966545

[35] M. A. Abuhussain, B. S. Alotaibi, M. S. Aliero, M. Asif, M. A. Alshenaifi, and Y. A. Dodo, "Adaptive HVAC System Based on Fuzzy Controller Approach", *Applied Sciences*, vol. 13, no. 20, Art. 11354, 2023. https://doi.org/10.3390/app132011354

[36] A. Beheshtikhoo, M. Pourgholi, and I. Khazaee, "Design of type-2 fuzzy logic controller in a smart home energy management system with a combination of renewable energy and an electric vehicle", *Journal of Building Engineering*, vol. 68, Art. 106097, 2023. https://doi.org/10.1016/j.jobe.2023.106097

[37] A. Chojecki, A. Ambroziak, and P. Borkowski, "Fuzzy Controllers Instead of Classical PIDs in HVAC Equipment: Dusting Off a Well-Known Technology and Today's Implementation for Better Energy Efficiency and User Comfort", *Energies*, vol. 16, no. 7, Art. 2967, 2023. https://doi.org/10.3390/en16072967

[38] J. M. Mendel and R. I. B. John, "Type-2 fuzzy sets made simple", *IEEE Transactions on Fuzzy Systems*, vol. 10, no. 2, pp. 117-127, 2002. https://doi.org/10.1109/91.995115

[39] N. N. Karnik, J. M. Mendel, and Q. Liang, "Type-2 fuzzy logic systems", *IEEE Transactions on Fuzzy Systems*, vol. 7, no. 6, pp. 643-658, 1999. https://doi.org/10.1109/91.811231

[40] ANSI/ASHRAE Standard 55-2023, Thermal Environmental Conditions for Human Occupancy. Atlanta, GA, USA: ASHRAE, 2023.

[41] ISO 7730:2005, Ergonomics of the thermal environment - Analytical determination and interpretation of thermal comfort using calculation of the PMV and PPD indices and local thermal comfort criteria. Geneva, Switzerland: International Organization for Standardization, 2005.

[42] EN 17037:2018, Daylight in buildings. Brussels, Belgium: European Committee for Standardization, 2018.

[43] ISO 3382-3:2012, Acoustics - Measurement of room acoustic parameters - Part 3: Open plan offices. Geneva, Switzerland: International Organization for Standardization, 2012.

[44] K. Deb, A. Pratap, S. Agarwal, and T. Meyarivan, "A fast and elitist multiobjective genetic algorithm: NSGA-II", *IEEE Transactions on Evolutionary Computation*, vol. 6, no. 2, pp. 182-197, 2002. https://doi.org/10.1109/4235.996017

[45] J. Kennedy and R. Eberhart, "Particle swarm optimization", in *Proceedings of ICNN'95 - International Conference on Neural Networks*, 1995, pp. 1942-1948. https://doi.org/10.1109/ICNN.1995.488968

[46] M. Dorigo and L. M. Gambardella, "Ant colony system: A cooperative learning approach to the traveling salesman problem", IEEE *Transactions on Evolutionary Computation*, vol. 1, no. 1, pp. 53-66, 1997. https://doi.org/10.1109/4235.585892

[47] V. Bulgakov, S. Pascuzzi, S. Ivanovs, V. Nadykto, and J. Nowak, "Kinematic discrepancy between driving wheels evaluated for a modular traction device", *Biosystems Engineering*, vol. 196, pp. 88-96, 2020. https://doi.org/10.1016/j.biosystemseng.2020.05.017

[48] R. Proot-Lafontaine, A. Merabtine, G. Henriot, and W. Maref, "Assessment and enhancement of indoor environmental quality in a school building", *Sustainability*, vol. 17, no. 12, Art. 5576, 2025. https://doi.org/10.3390/su17125576

[49] M. Miri et al., "Impact of indoor environmental quality on students' attention and relaxation levels during lecture-based instruction", *Buildings*, vol. 15, no. 16, Art. 2813, 2025. https://doi.org/10.3390/buildings15162813

[50] S. Sharov, S. Tereshchuk, A. Tereshchuk, V. Kolmakova, and N. Yankova, "Using MOOC to Learn the Python Programming Language", *International Journal of Emerging Technologies in Learning*, vol. 18, no. 02, pp. 17-32, 2023. https://doi.org/10.3991/ijet.v18i02.36431

[51] H. W. Brink, W. P. Krijnen, M. G. L. C. Loomans, M. P. Mobach, and H. S. M. Kort, "Positive effects of indoor environmental conditions on students and their performance in higher education classrooms: A between-groups experiment", *Science of the Total Environment*, vol. 868, Art. 161813, 2023. https://doi.org/10.1016/j.scitotenv.2023.161813

[52] *International Energy Agency*, Energy Efficiency 2024. Paris, France: IEA, 2024.